



Diminution of fluoride from groundwater using electrocoagulation: process optimization and role of arsenic interference

Vishakha Gilhotra, Rekha Yadav, Manpreet S Bhatti*

Department of Botanical and Environmental Sciences, Guru Nanak Dev University, Amritsar, Punjab, India, emails: mbhatti73@gmail.com/mbhatti.dobes@gndu.ac.in (M.S. Bhatti), vishgilhotra@gmail.com (V. Gilhotra), rekha1994.gndu@gmail.com (R. Yadav)

Received 22 September 2019; Accepted 31 March 2020

ABSTRACT

The global incidence of high fluoride levels in groundwater and its role in various health complications necessitate the development of effective methods for its reduction to sustainable limits. Thus, this study proposed an electrocoagulation technology of fluoride removal from groundwater. The groundwater having 4 mg/L fluoride was collected at 70 m depth from Khalra village (31.3955°N, 74.6211°E), Tarn Taran district, Punjab, India. Analysis of fluoride concentration was carried out using ion-chromatography. The central composite design (CCD) was employed to optimize the effect of treatment time and current density. Permissible fluoride concentration (1.5 mg/L) in drinking water was achieved at pH 7.4, treatment time 37 min, and current density 40 A/m² using aluminum electrodes with 1.64 kWh/m³ of energy consumption. The fluoride removal follows the pseudo-first-order kinetic model. Negative values of zeta potential indicated OH⁻ surface exchange mechanism of fluoride. Boehmite AlO(OH) formation in sludge was confirmed using X-ray diffraction. Fourier-transform infrared spectroscopy and Raman spectroscopy of sludge revealed that complex formation between aluminum hydroxide/oxyhydroxide and fluoride is crucial for removal.

Keywords: Groundwater; Ion-chromatography; Design of experiments (DOE); Response surface methodology (RSM); Arsenic interference

1. Introduction

The presence of various naturally occurring, anthropogenic, industry originated ions, and heavy metals profoundly affect the groundwater quality and give rise to human diseases. Fluoride is one such significant inorganic pollutant, has been acknowledged as a global concern. Fluoride is required in drinking water for the prevention of tooth cavities and mineralization of bones at the desired concentration [1], higher concentration and long term exposure can cause skeletal fluorosis, bone fracture, teeth mottling, and also in some cases, infertility in women [2]. The World Health Organization (WHO) and the Bureau of Indian Standards (BIS) have set the maximum acceptable limit of fluoride at 1.5 and 1 mg/L, respectively [3,4].

Fluoride contamination in groundwater has affected various south and southeastern Asian countries such as Afghanistan, Bhutan, Nepal, Sri Lanka, and India [5]. The high concentrations of fluoride have been reported in India (2.3–37.1 mg/L) [6] and Pakistan (5.5–29.6 mg/L) [7], along with considerable effects on human health. In India, 20 out of 29 states exceeds permissible level of fluoride in groundwater, including Assam (1.5–20.6 mg/L), Andhra Pradesh (1.5–8.2 mg/L), Haryana (1.5–17 mg/L), and Punjab (1.5–11.3 mg/L) [8]. As per the Central Ground Water Board (CGWB) report [9], a high concentration of fluoride and arsenic has been reported in groundwater of Punjab. In literature, many techniques have been reported to treat fluoride in groundwater, such as adsorption [10,11], coagulation-precipitation using aluminum salt [12],

* Corresponding author.

nanofiltration/reverse osmosis [13] and ion exchange [14]. However, these technologies have their own drawbacks. In adsorption based technologies, pH dependency and high treatment time are the significant obstacles in fluoride removal. Coagulation-precipitation with aluminum salts produces enormous amounts of sludge with high aluminum content [5]. Although nanofiltration and reverse osmosis are efficient in fluoride removal, it has certain limitations such as high maintenance and capital cost, fouling of membrane, high water rejection rate, which contains toxic pollutants. It removes some essential minerals from water, thus a re-mineralization process is also required [15].

In contrast to the technologies mentioned above, electrocoagulation (EC) is proven to be highly effective for the treatment of water [16,17]. It exhibits several advantages such as high removal efficiency, quick start-up, less generation of secondary pollutants, no chemical requirement, and less water rejection rate. EC uses several electrode materials such as iron [18], stainless steel [19], aluminum [20], and zinc [21]. Out of these iron and aluminum are widely used to treat different contaminants such as fluoride [22], arsenic [23,24], COD and turbidity [25], and hexavalent chromium [26]. These electrode materials are non-toxic, easily available, cost-effective, and anodically soluble, thus perform the combined task (EC+ electroflotation) and provide high removal efficiency [27]. The sludge generated in EC is low and less toxic as compared to other conventional technologies. However, at large scale, sludge disposal may become an issue. The possible uses of sludge are recycling (use as adsorbent or coagulant for subsequent wastewater treatment), coagulant recovery (using acidification or alkalization), and as building material [28].

Various studies are available on the removal of fluoride from groundwater by applying EC [17,23,24]. An integrated EC and microfiltration process was employed to treat fluoride contaminated groundwater collected from Assam, India, and maximum removal was observed at pH 7.9 and 15 A/m² [29]. Simultaneous removal of arsenic and fluoride from real groundwater of Durango, Mexico [18], and Chhattisgarh, India [19] using EC has also been reported. Optimization of process parameters of an EC reactor for fluoride removal from natural volcanic underground water has been performed. Three different reactors were employed, and fluoride concentration of 1.4 mg/L was obtained at 10 min and 100 A/m² [30].

Most of the experiments which have been performed so far or/and are being investigated to study the removal process of a particular pollutant only depict removal efficiency by maintaining certain factors constant and do not observe the combined effect of all the factors involved. This is time-consuming and requires a large number of experiments to determine optimum levels for various constants. These limitations can be eliminated by optimizing all the affecting variables simultaneously by statistical experimental design, such as response surface methodology (RSM). It is a statistical and mathematical tool which is used for model building and designing of small sets of experiments [31]. Central composite design (CCD) is a systematic experimental approach of RSM, in which combinations of factors (independent variables) are generated to find optimal solutions for maximization or minimization of the

response (dependent variable). This approach reveals the confounded 2-factor interaction (2-FI) between the independent variables, and it also shows whether the interactions are synergistic or antagonistic.

The study aims to optimize the process parameters (electrode material, pH, current density, and treatment time) for the removal of fluoride from simulated and real groundwater using CCD. The defluoridation kinetics and sludge characteristics were also studied to explore the removal mechanism. Furthermore, the interference of arsenic in the removal of fluoride by spiking of 300 ppb arsenic in real groundwater sample was also examined.

2. Materials and methods

2.1. Solutions

Analytical grade chemicals were used in the study. The stock solution of fluoride (100 ppm) was prepared by dissolving 0.221 g of NaF (Himedia, India) in 1,000 mL ultrapure water. Working fluoride solution of 5 mg/L was prepared by diluting the stock solution. The pH was adjusted using 1 N HCl and 1 N NaOH solution. Sodium chloride (Merck, India) was used to set the conductivity (2,000 μ S/cm) of the synthetic sample. The arsenic solution of 300 ppb was prepared by adding an appropriate amount of NaAsO₂ (Merck, India) in ultrapure water.

2.2. Groundwater characterization

Groundwater sample of fluoride was collected from a tube-well at a depth of 70 m located in the Khalra village (31.3955°N, 74.6211°E) Tarn Taran, Punjab (Fig. 1, Table S1). The sample was collected in the pre-rinsed high-density polyethylene (HDPE) bottle after 10 min of initial pumping. The health effects of high concentrations of fluoride in the groundwater among inhabitants, such as skeletal fluorosis and mottling of teeth, were also observed (Fig. S1). The characteristics of the groundwater sample were pH 7.4, fluoride 4.0 mg/L, chloride 66 mg/L, sulfate 168 mg/L, total hardness 264 mg/L as CaCO₃, total alkalinity 570 mg/L as CaCO₃, and conductivity 2,100 μ S/cm.

2.3. Analytical methods

pH and conductivity of the sample were measured using digital pH meter (Labtronics, LT-501, India) and conductivity meter (Labtronics, LT-51, India). Anions (fluoride, chloride, and sulfate) were analyzed using ion chromatography (IC 883, Metrohm, Switzerland). Total hardness of the sample was evaluated using ethylenediaminetetraacetic acid titrimetric method, and total alkalinity was analyzed by the titration method using H₂SO₄ within 24 h of sampling as per standard method [32].

2.4. EC reactor design

EC experiments in the batch mode were conducted in 1,000 mL Plexiglas reactor containing a working volume of 540 mL and dimensions of 7 cm × 4 cm × 40 cm. A pair of electrodes was used with an effective surface area of

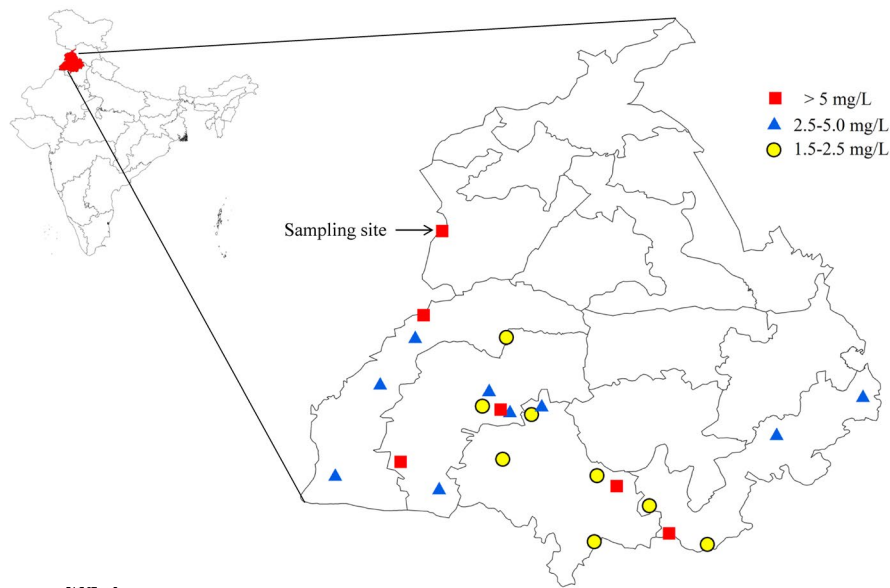


Fig. 1. Map showing fluoride in groundwater of Punjab, India as per CGWB report [9].

100 cm². Electrodes were rubbed with sandpaper (120 grit) and cleaned with tap water before use. A stabilized DC power supply (L-3210, Aplab, India) was connected with an inter-electrode distance of 15 mm. Magnetic stirrer was used for continuous mixing of the sample at 100 rpm. EC reactor design and reaction mechanism are shown in Fig. 2. After EC treatment, the sample was maintained under quiescent conditions for 30 min and filtered through a 0.2 μm membrane filter to avoid choking of the anion column. Fluoride removal efficiency and energy consumption were calculated as per Eqs. (1) and (2), respectively:

$$\text{Fluoride removal (\%)} = \frac{C_i - C_t}{C_i} \times 100 \quad (1)$$

where C_i and C_t are the initial and final concentrations of fluoride, respectively.

$$\text{Energy (kWh/m}^3\text{)} = \frac{\text{voltage (V)} \times \text{current (I)} \times \text{treatment time (t)}}{\text{Functional volume (v)}} \quad (2)$$

The schematic flow chart of the work done is shown in Fig. 3. Preliminary experiments were performed using simulated fluoride (5 mg/L) for the best electrode material. The experiments were performed at pH 7, current density 10 A/m², and treatment time varied between 5 and 35 min using each electrode material (iron, aluminum, and stainless steel). The best electrode material was further used to treat real groundwater. The effect of treatment time (3–37 min) and current density (10–40 A/m²) on fluoride removal was analyzed using 2-factor CCD design at natural pH and conductivity. The sample treated at optimized parameters was considered for removal kinetic study and sludge characterization.

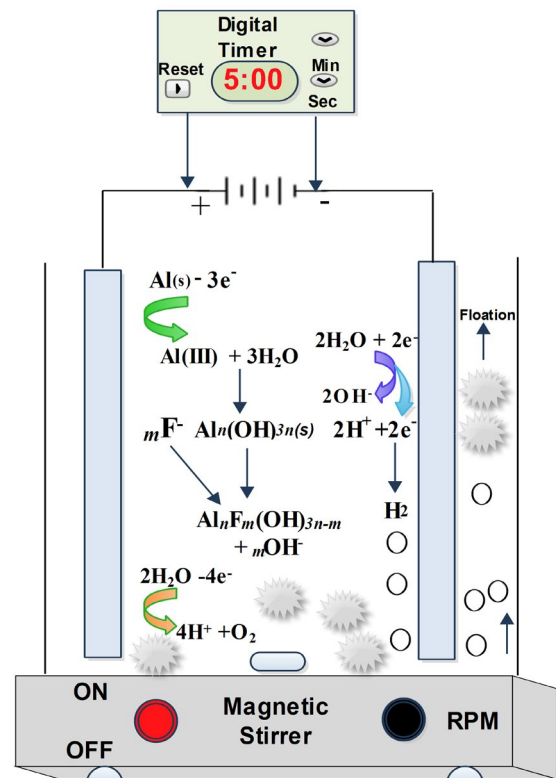


Fig. 2. Electrocoagulation experimental setup.

2.5. CCD design and optimization

To study the significant process variables viz. treatment time 3–37 min, current density 10–40 A/m², 13 experiments were performed at factorial, axial, and center points as per CCD-RSM approach (Table 1). Fluoride removal efficiency and energy consumption were determined as response

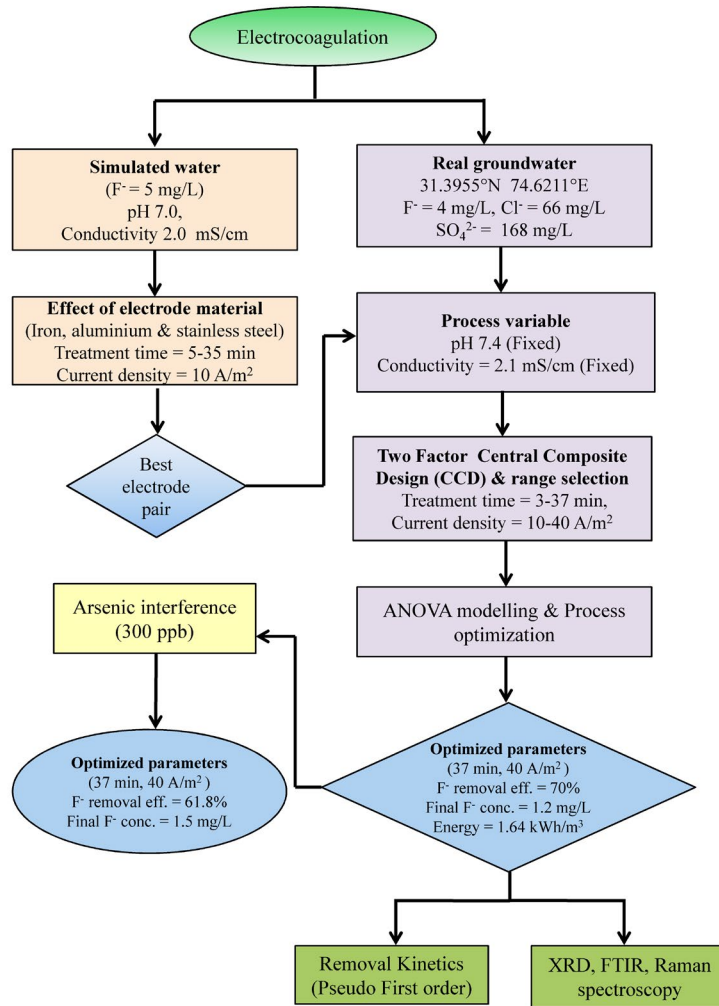


Fig. 3. Flow chart of experimental procedure and optimized conditions.

Table 1
Two-factor CCD of real groundwater sample with fluoride removal efficiency and energy consumption

		Independent variables		Responses (observed)		
		X_1 (min)	X_2 (A/m ²)	Y_1 (%)	Y_2 (kWh/m ³)	Y_3 (%)
1	Factorial	3	10	3.2	0.018	2.5
2	Factorial	3	40	24.7	0.144	25.0
3	Factorial	37	10	42.0	0.227	38.0
4	Factorial	37	40	70.0	1.774	61.8
5	Axial	3	25	20.0	0.053	18.5
6	Axial	20	10	18.7	0.123	15.5
7	Axial	20	40	43.5	0.959	43.2
8	Axial	37	25	62.0	0.649	55.0
9	Center	20	25	39.0	0.351	39.0
10	Center	20	25	39.3	0.351	38.0
11	Center	20	25	40.0	0.351	39.0
12	Center	20	25	41.0	0.351	40.0
13	Center	20	25	41.0	0.351	39.5

X_1 = Treatment time; X_2 = Current density; Y_1 = Fluoride removal efficiency
 Y_2 = Energy consumption; Y_3 = Fluoride removal eff. in presence of 300 ppb arsenic

variables and used for ANOVA model building. Model statistics (coefficient of variance (CV) %, predicted R^2 , adequate precision) along with the normal plot of residuals and predicted vs. actual plot of response were checked for outlier and goodness of fit. The fitted model was selected on the basis of p -value (p -value < 0.05) and non-significant lack of fit (p -value > 0.05). The best-fitted model was used for a graphical representation (2-dimensional and 3-dimensional contour plots) of the response variables with respect to treatment time and current density. Design-Expert v9.06 (Stat-Ease Inc., USA) was used for experimental design and data analysis.

2.6. Zeta (ζ) potential

Treated samples after filtration were analyzed for ζ -potential measurement by zeta meter (Zetasizer Nano S90, Malvern instruments Ltd., UK). A gold electrode was used to determine the effective charge of the particle, which gives a direct indication of the stability of the solution.

2.7. Sludge characterization

To elucidate the mechanism of defluoridation, sludge samples were oven-dried and grained into a fine powder. XRD of samples was recorded using X-ray diffractometer (XRD-6100/7000, Shimadzu) with Cu $K\alpha$ radiation (1.541 Å) in the range of 5° to 90° to check the crystalline nature and mineralogical structure of sludge. Peaks were analyzed from the published literature and International Centre for Diffraction Data (ICDD) database.

Scanning electron microscopy (SEM) analysis was carried out for visual information of change in morphology of sludge particles at a magnification of 2,000×. Fourier transform infrared spectroscopy (FTIR) study was performed for the analysis of chemical groups and bond stretching in the sludge particles (Perkin Elmer, USA). Potassium bromide (KBr) was used for floc sample preparation, and the range of spectra was 4,000–400 cm^{-1} . Raman spectroscopy was used to identify materials from their bonding. Raman spectroscopy of sludge samples was performed using the Renishaw In-Via micro-Raman spectrometer with 50 mW argon laser (785 nm) as excitation radiation, and the resolution of the spectra was 1 cm^{-1} .

3. Results and discussion

Treatment of simulated water sample was performed to check the effect of electrode material on fluoride removal efficiency. In the first phase, three-electrode material iron, aluminum, and stainless steel were used and the best electrode pair was used for further treatment. In the second phase, the real groundwater sample was taken from bore well (70 m depth). Process parameters viz. pH and conductivity were not altered and kept fixed. Significant process variables viz. treatment time and current density were optimized using CCD-RSM approach.

3.1. Effect of electrode material using simulated water

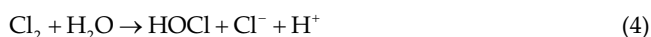
The maximum fluoride removal efficiency was obtained with Al–Al electrodes (94.4%) and lowest with SS–SS electrodes (59.3%) at pH 7, treatment time 35 min, and current

density 10 A/m² (Fig. S2). This may be due to the tendency of fluoride making a strong complex with aluminum by chemical adsorption process in which F⁻ is replaced by OH⁻ from aluminum oxide hydroxide flocs [25,33]. Therefore, poorly soluble aluminum fluoride hydroxide forms settle as sludge, as shown in Fig. 2. Aoudj et al. [25] used five different anode configurations viz. four aluminum (4-Al), three aluminum-one iron (3Al-1Fe), two aluminum-two iron (2Al-2Fe), three iron-one aluminum (3Fe-1Al), and four iron (4-Fe) and maximum fluoride removal efficiency was obtained with 4-Al configuration. Thus, due to better removal efficiency, the Al–Al electrode pair was further used for real groundwater treatment.

3.2. Process parameters for real groundwater

According to the literature, the optimum pH for fluoride removal is 6–7 [22,33]. At highly acidic pH, the dissolution rate of aluminum is low, and hydroxide ions produced during the reaction get utilized by the acid in solution [27]. At highly alkaline pH, soluble aluminum hydroxide/oxide species such as Al(OH)₄⁻ and AlO₂⁻ are predominant with a poor coagulating capacity [34]. However, at neutral pH, the formation of gelatinous aluminum oxide hydroxide AlO(OH) (boehmite) is predominant, and the surface of AlO(OH) contains crystalline structured hydroxyl groups, which further provide excellent adsorption capacity for fluoride ions [35].

The conductivity of the sample determines the resistance of the electrochemical cell, a high amount of chloride ions diffuses the oxide layer around the electrode and increases the corrosion of electrodes, which in turn decreases the resistance. In the presence of chloride ions, reactions (3)–(5) occur at anode [36].



With an increase in the concentration of NaCl, the voltage decreases rapidly due to the ohmic potential drop and reduces the anode overpotential. Thus localized outbreak of passive layer occurs, known as “pitting corrosion,” which accelerates the fluoride removal efficiency by producing more coagulants. The presence of pits on the anode and their size depends on the concentration of NaCl. With an increase in concentration, the finer pits form with high distribution density [37,38]. The energy consumption gets significantly reduced with an increase in conductivity of the sample due to a decrease in ohmic resistance between the electrodes [33]. Therefore, all the experiments were performed using natural pH 7.4 and conductivity 2,000 $\mu\text{S}/\text{cm}$ of groundwater.

3.3. Process modeling and optimization

Groundwater sample was treated according to 2-factor CCD with current density and treatment time as process

variables. The fluoride removal efficiency and energy consumption as a response variable are listed in Table 1. Best model fitting of response data (Fluoride removal efficiency) indicated a quadratic model with a highly significant p -value < 0.0001 at F -value = 555.1. Model has non-significant Lack of fit ($p = 0.2212$, p -value > 0.05 indicated S/N ratio = 84.73) (Tables 2a and b). The normal percentage probability (Fig. S3) and actual vs. predicted plot (Fig. 4a) suggested model precision and reliability for the prediction of fluoride removal efficiency. Thus, the model can be navigated in the design space, and the developed model can efficiently predict fluoride removal efficiency.

Treatment time and current density are two important variables as these influence the reaction rate, production, growth, and dose of coagulants. Fluoride removal efficiency is directly proportional to the coagulant (aluminum

hydroxide/oxide) dosage rate [39]. Due to an increase in treatment time and current density, Al^{3+} ion production rate, and size of flocs increase, which eventually neutralizes the charged pollutant particles. Therefore, it significantly increases the fluoride removal efficiency. The effect of current density was predominant at lower values, that is, 10 and 25 A/m^2 . The increase in fluoride removal efficiency from 10 to 25 A/m^2 at 37 min was 20%, while from 25 to 40 A/m^2 was only 8%. The lower removal rates might be due to the fact that high current density leads to the liberation of aluminum hydroxide $Al(OH)_3$ and cause the incomplete reaction [30,35]. The minimum fluoride removal efficiency of 3.25% was observed at 3 min and 10 A/m^2 . This may be due to the insufficient production of coagulants to remove fluoride ions. The maximum removal efficiency of fluoride (70%) was observed at a

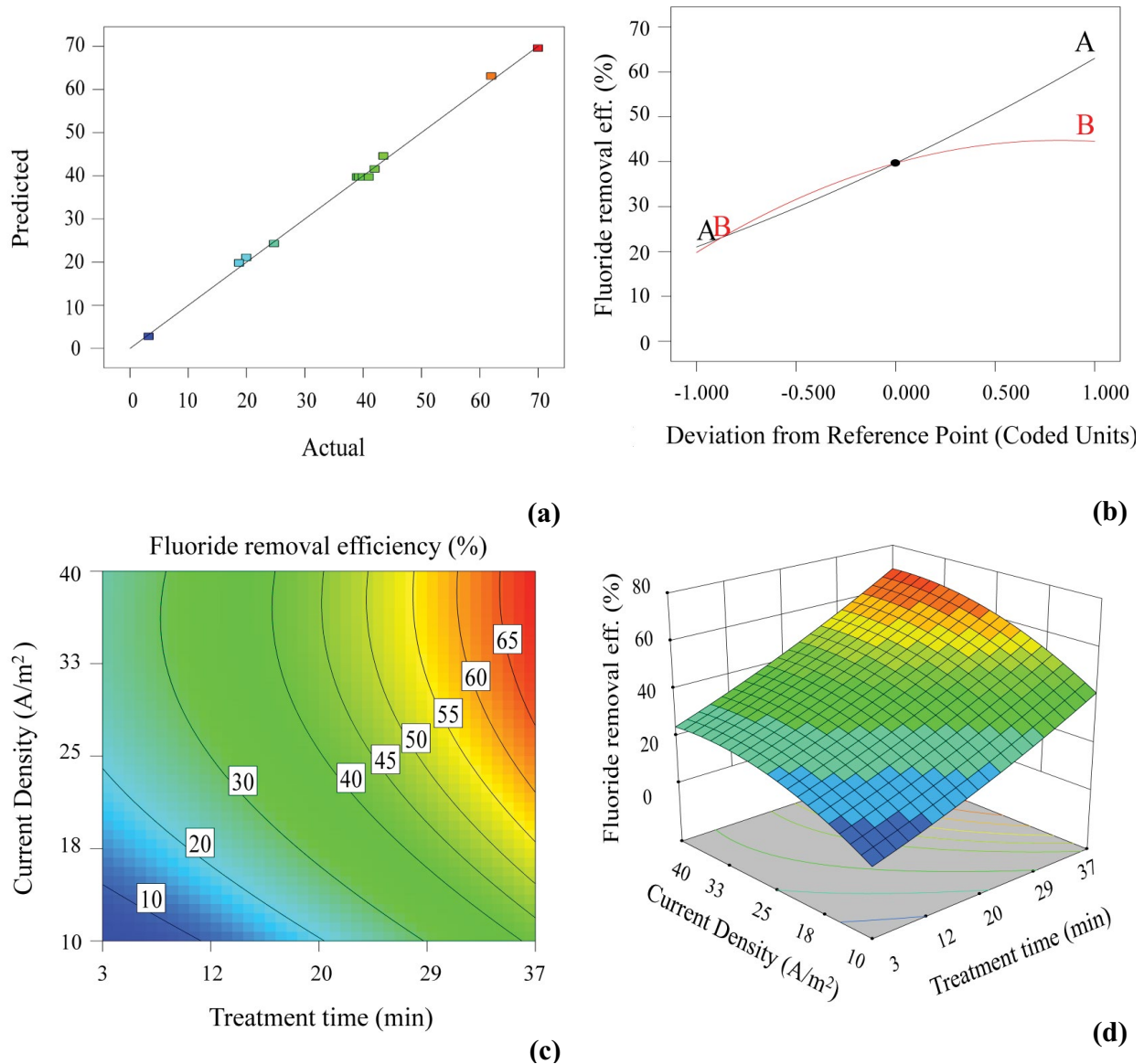


Fig. 4. (a) Actual vs. predicted, (b) perturbation plot, (c) 2-D contour, and (d) 3-D contour plots showing the effect of treatment time and current density on fluoride removal efficiency.

Table 2

ANOVA table and model statistics for (a) fluoride removal efficiency, (b) fluoride removal efficiency in presence of 300 ppb arsenic, and (c) second-order polynomial equations for fitted models

(a)

Source	SS ^a	Df ^b	MS ^c	F-value	p-value Probability > F
Model	3,732.3	5	746.4	555.1	<0.0001*
A	2,646.0	1	2,646.0	1,967.7	<0.0001*
B	918.8	1	918.8	683.3	<0.0001*
A × B	10.5	1	10.5	7.8	0.0264*
A ²	15.3	1	15.3	11.4	0.0118*
B ²	156.1	1	156.1	116.0	<0.0001*
Lack of fit	5.9	3	1.9	2.2	0.2212 [‡]

Model statistics

Standard deviation	1.1	R ²	0.997
Mean	37.2	Adjusted R ²	0.995
% CV	3.1	Predicted R ²	0.987
PRESS	45.5	Adequate precision	84.73

(b)

Source	SS	Df	MS	F-value	p-value Probability > F
Model	4,974.4	5	994.8	141.0	<0.0001*
A	3,002.5	1	3,002.5	425.6	<0.0001*
B	1,596.2	1	1,596.2	226.3	<0.0001*
A × B	3.2	1	3.2	0.4	0.5089
A ²	21.9	1	21.9	3.1	0.1052
B ²	63.2	1	63.2	8.9	0.0122
Lack of fit	65.8	9	7.3	1.2	0.5228 [‡]

Model statistics

Standard deviation	2.6	R ²	0.984
Mean	31.0	Adjusted R ²	0.977
% CV	8.5	Predicted R ²	0.966
PRESS	170.9	Adequate precision	38.219

*Significant at $p \leq 0.05$.[‡]Not-significant at $p < 0.05$.^aSS = Sum of squares; ^bDf = Degree of freedom; ^cMS = Mean sum of squares.

A = Treatment time; B = Current density.

(c)

Response	Term	Equation
Y ₁ (%)	Coded	+39.66 + 21.00 A + 12.37 B + 1.63 A × B + 2.36 A ² – 7.52 B ²
	Actual	–20.110 + 0.749 A + 2.368 B – 0.006 A × B – 0.008 A ² – 0.033 B ²
Y ₃ (%)	Coded	+33.98 + 18.31 A + 11.84 B – 0.66 A × B + 2.67 A ² – 4.29 B ²
	Actual	–16.79 + 0.772 A + 1.793 B – 0.0260 A × B + 0.0924 A ² – 0.019 B ²

Coded (A = Treatment time, B = Current density in coded units).

Actual (A = Treatment time in min, B = Current density in A/m² in actual units).Y₁ = Fluoride removal efficiency; Y₃ = Fluoride removal efficiency in presence of 300 ppb arsenic.

treatment time of 37 min and a current density of 40 A/m² with a residual fluoride concentration of 1.2 ppm, which is below the WHO limit of fluoride in drinking water. The interaction between two variables (treatment time and current density) is clearly shown by the perturbation plot, 2D, and 3D contour plot (Figs. 4b–d). Energy consumption is an essential parameter in terms of the practical applicability of the EC technique at the community level. For energy consumption, the quadratic model with *p*-value < 0.0001 and *F*-value = 106.7 implied the fitting of the second-order polynomial model to the experimental data. The model revealed that current density is the most critical factor responsible for energy consumption.

In the optimization process, desirability plots (Fig. S4) revealed that the maximum removal efficiency was obtained under optimum values of treatment time (37 min) and current density (40 A/m²) with energy consumption of 1.64 kWh/m³.

The second-order polynomial equations for fluoride removal efficiency and energy consumption as coded and actual factors are given in Table 2c. It has been observed that complete removal of fluoride from simulated water was achieved at pH 7, current density 10 A/m² within 37 min of treatment time. EC treatment up to 37 min observed negligible change in the chloride and sulfate concentrations, whereas fluoride was removed up to 70% for real water sample (Fig. S5). This indicated that coexistence of ions like chloride and sulfate significantly reduces fluoride removal efficiency.

3.4. Fluoride removal kinetics

The rate of removal of fluoride is explained by a pseudo-first-order kinetics model Eq. (6):

$$\frac{dC_t}{dt} = kC_t C_{Ad} \quad (6)$$

where *k*, *C_t*, and *C_{Ad}* are the rate constant (min⁻¹), concentration of fluoride at *t* time, and concentration of adsorbent (aluminum oxide hydroxide), respectively. At a fixed current density, the amount of adsorbent is assumed to be unchanged. Thus, the simplified form of equation will be Eq. (7):

$$\frac{dC_t}{dt} = kC_t \quad (7)$$

After integration, Eq. (7) gives Eq. (8):

$$-\ln \frac{C_t}{C_i} = -kC_t \quad (8)$$

where *C_i* is influent fluoride concentration.

The value of *k* can be calculated from the slope of the graph between $-\ln(C_t/C_i)$ vs. time (Fig. 5a). As shown in Fig. 5b, the value of *k* increases (0.0064–0.0098 min⁻¹) as current density changes from 10 to 40 A/m². At high current density, the increased production of in-situ coagulants leads to a rise in the rate constant [24].

3.5. Zeta-potential

The zeta (ζ) – potential of samples treated at different times in the absence (simulated water with no fluoride) and presence (real groundwater) of fluoride was determined (Fig. 6). The initial pH of the sample was 7.4. In the absence of fluoride, the positive values of ζ – potential were observed. At the duration of 10 min, maximum ζ – potential was obtained. As the aluminum dissolution at anode increases, a point is reached where a sudden rise in ζ – potential was observed, passing through the isoelectric point. After 10 min, ζ – potential started to decline due to an increase in sample pH. In the presence of F⁻ ions, negative values of ζ – potential can be justified by the reported OH⁻ surface-exchange mechanism of adsorption of fluoride onto aluminum oxide hydroxide. In surface exchange reaction, F⁻ ions get exchanged with OH⁻ ions and surface become negatively charged [17] as shown in Eq. (9):



This surface exchange reaction suggested that fluoride chemisorbs onto boehmite as adsorption occurs on the negatively charged surface [40].

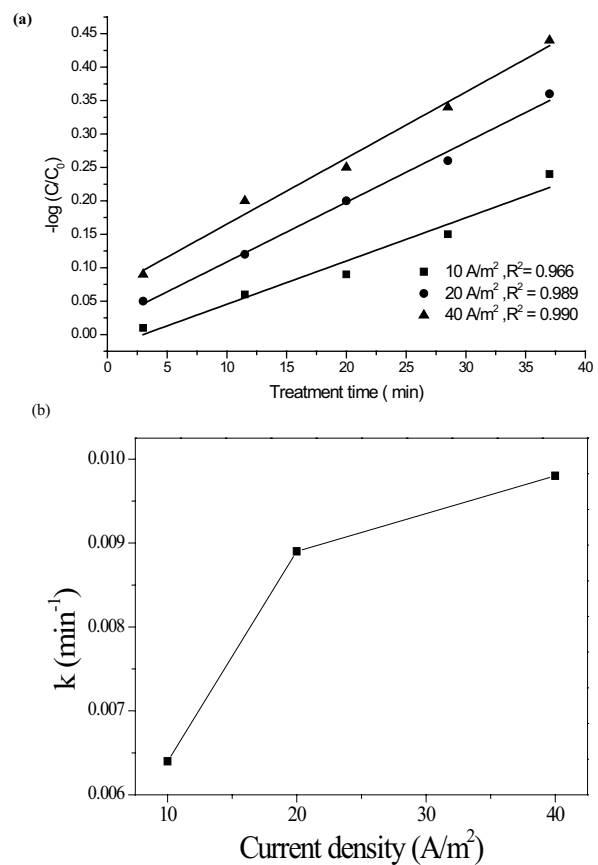


Fig. 5. (a) Pseudo-first-order kinetic model plot and (b) rate constants for fluoride removal at different current density.

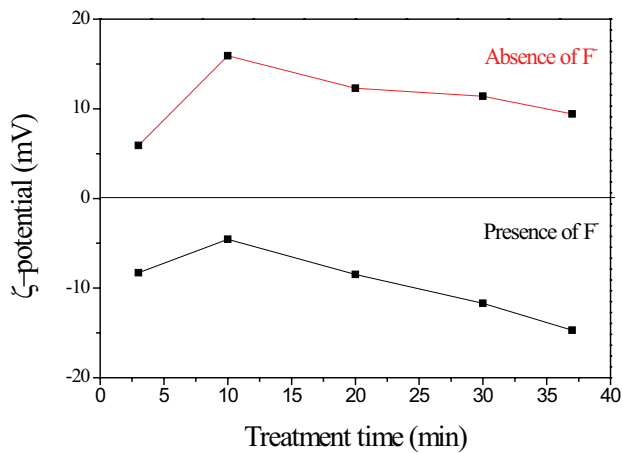


Fig. 6. Variation of zeta potential with treatment time in (a) absence of fluoride and (b) real groundwater sample.

3.6. Sludge characterization

3.6.1. XRD and SEM analysis

XRD analyzed the mineral composition and crystalline structure of EC sludge in the absence (simulated water with no fluoride) and presence (real groundwater) of fluoride. As represented in Fig. 7a in the absence of fluoride, diffraction peaks at $2\theta = 14.47^\circ, 28.18^\circ, 38.9^\circ, 49.6^\circ, 64.8^\circ, 66.5^\circ,$ and 71.9° indicated the generation of boehmite (aluminum hydroxide oxide, $\text{AlO}(\text{OH})$) (JCPDS: 83–2384). However, in fluoride-treated sludge, diffraction peaks at $2\theta = 26.32^\circ, 27.16^\circ,$ and 38.89° are due to the aluminum oxide fluoride (JCPDS: 76–2058) and peaks at $2\theta = 33.14^\circ, 38.48^\circ, 45.9^\circ, 64.36^\circ,$ and 77.5° suggested the formation of aluminum oxide (Al_2O_3) (JCPDS: 02–1114). The results are in consonance with published literature [30]. SEM analysis revealed that in the absence of fluoride, fine particles were present on the surface (Fig. 7b). While in the presence of fluoride, floc size increased with agglomeration,

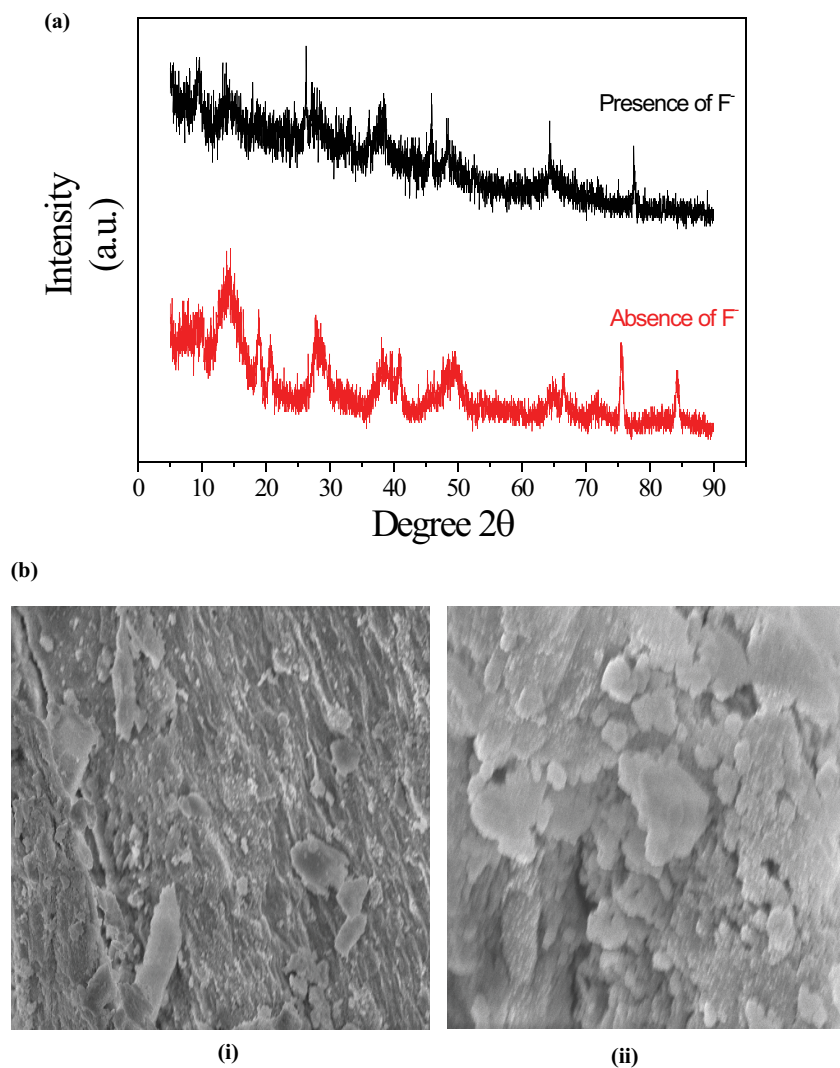


Fig. 7. (a) XRD and (b) SEM analysis of sludge in the (i) absence of fluoride and (ii) real groundwater sample.

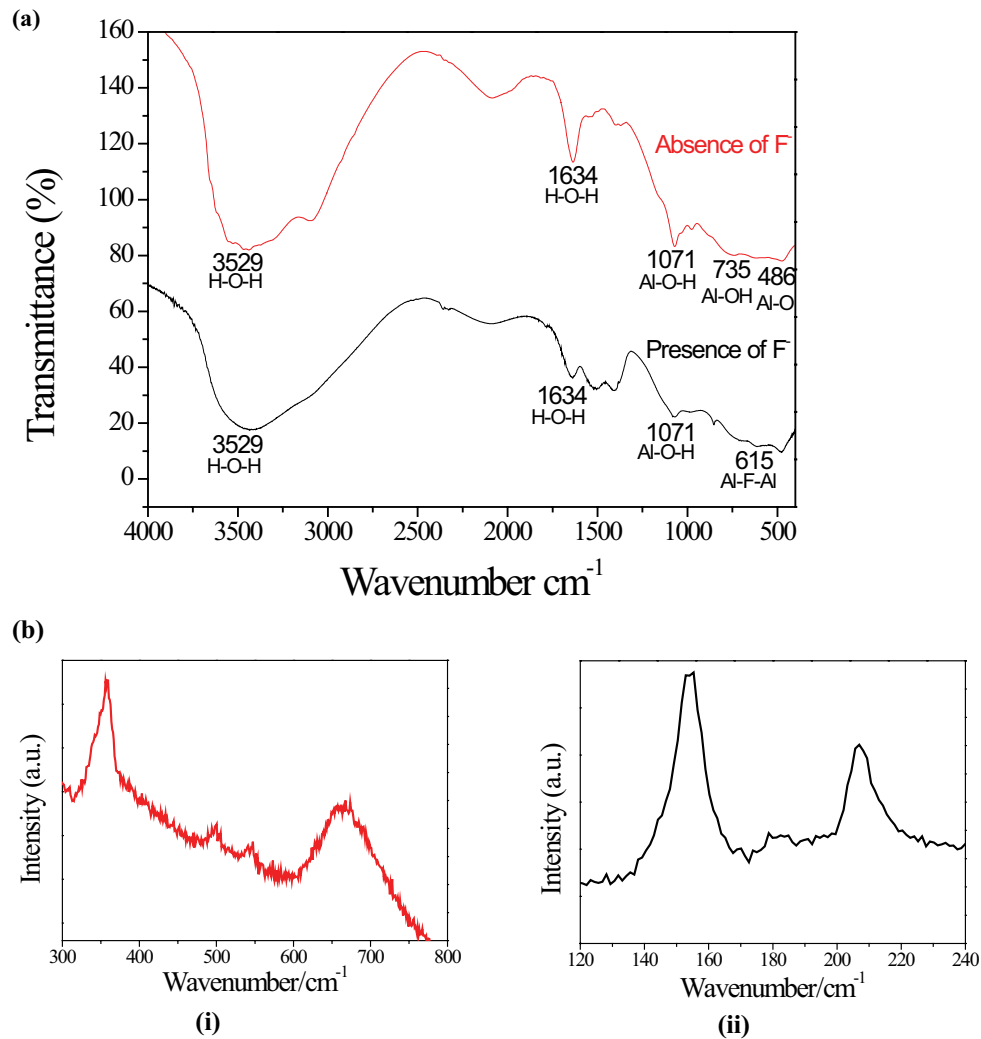


Fig. 8. (a) FTIR and (b) Raman spectra of sludge in the (i) absence of fluoride and (ii) real groundwater sample.

complexation, and destabilization of fluoride ions with aluminum oxide hydroxide (Fig. 7c).

3.6.2. FTIR and Raman spectroscopy

FTIR spectrum in the absence (simulated water with no fluoride) and presence (real groundwater) of fluoride is shown in Fig. 8a. Spectra bands at 3,529; 1,634; 1,071; 735; and 486 were observed in the absence of fluoride. Broadbands observed at 3,529 and 1,634 cm^{-1} were attributed to the H–O–H stretching and bending vibrations, respectively [40]. A peak at 1,071 cm^{-1} indicated the stretching of Al–O–H bond [2]. The band at 735 cm^{-1} could be assigned to Al–OH (torsional) and at 486 cm^{-1} corresponded to Al–O (stretching) in the boehmite octahedral structure [41]. Similar band patterns were observed in the presence of fluoride except for the bands at 615 and 477 cm^{-1} . The 615 cm^{-1} peak could be attributed to Al–F–Al (stretching) [42]. FTIR spectra justify the substitution of the hydroxyl group by fluoride, and the results are in agreement with the published work [43].

Raman spectra of sludge samples in the absence and presence of fluoride is shown in Fig. 8b and c. In the absence of fluoride, bands observed in the range of 400–800 cm^{-1} were assigned to OH translation modes [44], and strong peaks at 498 and 359 cm^{-1} were assigned to the Al–O (stretching) bond indicated the formation of boehmite [45]. However, in the presence of fluoride, two peaks observed in the region of 100–200 cm^{-1} were ascribed to the occurrence of dimeric binuclear fluoro-aluminate complexes with two or three F⁻ atoms [46].

3.7. Arsenic interference

In the presence of 300 ppb arsenic, the maximum fluoride removal efficiency of 61.85% was observed at 37 min and 40 A/m². However, in the absence of arsenic, 70% fluoride removal efficiency was achieved. The interference of arsenic was further analyzed by the response data obtained from the optimization of process variables (treatment time and current density). The reduction in fluoride removal efficiency in the presence of 300 ppb arsenic is 6%–8%

Table 3
Comparison of fluoride removal efficiency in the absence and presence of arsenic

X_1 (min)	X_2 (A/m ²)	Fluoride (mg/L)	Y_1 (%)	Fluoride in presence of arsenic (mg/L)	Y_3 (%)	$Y_1 - Y_3$ (change) (%)
20	10	3.0	24.5	3.1	18.0	6.50
37	10	2.1	45.2	2.3	39.6	5.61
20	25	2.4	39.6	2.4	33.0	6.51
37	25	1.4	63.0	1.6	55.0	7.96
20	40	2.0	50.0	2.2	41.5	8.49
37	40	1.2	70.0	1.5	61.8	8.15

X_1 = Treatment time; X_2 = Current density.

Y_1 = Fluoride removal efficiency; Y_3 = Fluoride removal efficiency in presence of 300 ppb arsenic.

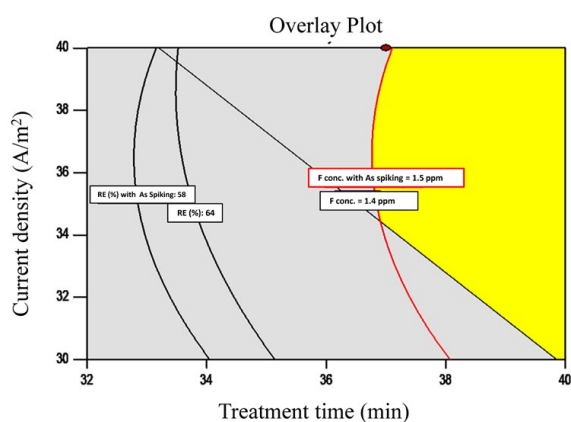


Fig. 9. Overlay plot showing the effect of arsenic interference on fluoride removal efficiency.

(Fig. 9). This may be due to the fact that the substitution of hydroxide radicals by F^- is reduced by adsorption of arsenic onto aluminum flocs, thus affecting fluoride removal efficiency [47]. It was observed that either by increasing treatment time from 20 to 37 min or current density from 10 to 40 A/m² fluoride removal efficiency increased by 21% (Table 3). Therefore, an increase in treatment time would be more economical as compared to current density as energy consumption will be lesser in the former.

4. Conclusions

Fluoride contaminated real groundwater was efficiently treated at optimized process conditions viz. pH 7.4, treatment time 37 min, and current density 40 A/m² using aluminum electrodes. Under the optimized conditions, the residual fluoride concentration in treated water was found to be 1.2 mg/L with energy consumption of 1.64 kWh/m³. Removal of fluoride in EC follows the pseudo-first-order kinetic model. Zeta potential study confirms the OH^- surface exchange mechanism of fluoride, in which F^- ions get exchanged with hydroxyl group from aluminum flocs. XRD, SEM, FTIR, and Raman spectroscopy analysis of sludge indicated the formation of a complex between Al^{3+} and F^- , which further confirms the removal of fluoride from water samples. The coexistence of 300 ppb arsenic reduces the

fluoride removal efficiency by 6%–8%. Therefore, an increase in treatment time would be more economical as compared to current density to achieve maximum fluoride removal efficiency.

Acknowledgments

MSB is thankful to the University Grants Commission, New Delhi for financial support under Major Research Project [43-314/2014(SR)]. Authors acknowledge UGC-UPE support for Ion-Chromatography and Zeta potential studies under Emerging Life Sciences, GNDU, Amritsar.

References

- [1] K.S. Hashim, A. Shaw, R. Al Khaddar, M.O. Pedrola, D. Phipps, Defluoridation of drinking water using a new flow column-electrocoagulation reactor (FCER)-experimental, statistical, and economic approach, *J. Environ. Manage.*, 197 (2017) 80–88.
- [2] K. Govindan, M. Raja, S.U. Maheshwari, M. Noel, Y. Oren, Comparison and understanding of fluoride removal mechanism in Ca^{2+} , Mg^{2+} and Al^{3+} ion assisted electrocoagulation process using Fe and Al electrodes, *J. Environ. Chem. Eng.*, 3 (2015) 1784–1793.
- [3] WHO, Guidelines for Drinking Water Quality: First Addendum to Volume 1, Recommendations, World Health Organization, Geneva, 2006.
- [4] BIS, Indian Standards-Drinking Water Specifications, IS10500, Bureau of Indian Standards, New Delhi, 2012.
- [5] K.K. Yadav, S. Kumar, Q.B. Pham, N. Gupta, S. Rezania, H. Kamyab, S. Yadav, J. Vymazal, V. Kumar, D.Q. Tri, A. Talaiekhazani, Fluoride contamination, health problems and remediation methods in Asian groundwater: a comprehensive review, *Ecotoxicol. Environ. Saf.*, 182 (2019) 109362.
- [6] S. Ali, Y. Fakhri, M. Golbini, S.K. Thakur, A. Alinejad, I. Parseh, S. Shekhar, P. Bhattacharya, Concentration of fluoride in groundwater of India: a systematic review, meta-analysis and risk assessment, *Groundwater Sustainable Dev.*, 9 (2019) 100224.
- [7] A. Rasool, T. Xiao, Z.T. Baig, S. Masood, K.M. Mostofa, M. Iqbal, Co-occurrence of arsenic and fluoride in the groundwater of Punjab, Pakistan: source discrimination and health risk assessment, *Environ. Sci. Pollut. Res. Int.*, 22 (2015) 19729–19746.
- [8] D. Chakraborti, M.M. Rahman, A. Chatterjee, D. Das, B. Das, B. Nayak, A. Pal, U.K. Chowdhury, S. Ahmed, B.K. Biswas, M.K. Sengupta, Fate of over 480 million inhabitants living in arsenic and fluoride endemic Indian districts: magnitude, health, socio-economic effects and mitigation approaches, *J. Trace Elem. Med. Biol.*, 38 (2016) 33–45.
- [9] CGWB, Groundwater Year Book of Punjab and Chandigarh (UT), Central Ground Water Board, Ministry of Water Resources,

- River Development and Ganga Rejuvenation, Government of India, 2016.
- [10] M. Mourabet, A. El Rhilassi, H. El Boujaady, M. Bennani-Ziatni, R. El Hamri, A. Taitai, Removal of fluoride from aqueous solution by adsorption on hydroxyapatite (HAp) using response surface methodology, *J. Saudi Chem. Soc.*, 19 (2015) 603–615.
- [11] Y. Yu, L. Yu, J.P. Chen, Adsorption of fluoride by Fe–Mg–La triple-metal composite: adsorbent preparation, illustration of performance and study of mechanisms, *Chem. Eng. J.*, 262 (2015) 839–846.
- [12] F. Venditti, F. Cuomo, G. Giansalvo, M. Giustini, G. Cinelli, F. Lopez, Fluorides decontamination by means of aluminum polychloride based commercial coagulant, *J. Water Process. Eng.*, 26 (2018) 182–186.
- [13] J. Shen, A.I. Schäfer, Factors affecting fluoride and natural organic matter (NOM) removal from natural waters in Tanzania by nanofiltration/reverse osmosis, *Sci. Total Environ.*, 527 (2015) 520–529.
- [14] Y.X. Zhang, Y. Jia, Fluoride adsorption on manganese carbonate: Ion-exchange based on the surface carbonate-like groups and hydroxyl groups, *J. Colloid Interface Sci.*, 510 (2018) 407–417.
- [15] S.V. Jadhav, E. Bringas, G.D. Yadav, V.K. Rathod, I. Ortiz, K.V. Marathe, Arsenic and fluoride contaminated groundwaters: a review of current technologies for contaminants removal, *J. Environ. Manage.*, 162 (2015) 306–325.
- [16] S. Aoudj, A. Khelifa, N. Drouiche, M. Hecini, Removal of fluoride and turbidity from semiconductor industry wastewater by combined coagulation and electroflotation, *Desal. Water Treat.*, 57 (2016) 18398–18405.
- [17] M.A. Sandoval, R. Fuentes, J.L. Nava, O. Coreño, Y. Li, J.H. Hernández, Simultaneous removal of fluoride and arsenic from groundwater by electrocoagulation using a filter-press flow reactor with a three-cell stack, *Sep. Purif. Technol.*, 208 (2019) 208–216.
- [18] S. Khaldia, H. Lounicia, M. Drouichea, N. Drouichea, Treatment of ointment pharmaceutical wastewater by electrocoagulation process, *Desal. Water Treat.*, 71 (2017) 152–158.
- [19] V. Gilhotra, L. Das, A. Sharma, T.S. Kang, P. Singh, R.S. Dhuria, M.S. Bhatti, Electrocoagulation technology for high strength arsenic wastewater: process optimization and mechanistic study, *J. Cleaner Prod.*, 198 (2018) 693–703.
- [20] T. Ouslimane, S. Aoudj, M. Amara, N. Drouiche, Removal of copper and fluoride from mixed Cu-CMP and fluoride-bearing wastewaters by electrocoagulation, *Int. J. Environ. Res.*, 11 (2017) 677–684.
- [21] F. Hussin, F. Abnisa, G. Issabayeva, M.K. Aroua, Removal of lead by solar-photovoltaic electrocoagulation using novel perforated zinc electrode, *J. Cleaner Prod.*, 147 (2017) 206–216.
- [22] M. Behbahani, M.A. Moghaddam, M. Arami, Techno-economical evaluation of fluoride removal by electrocoagulation process: optimization through response surface methodology, *Desalination*, 271 (2011) 209–218.
- [23] A. Guzmán, J.L. Nava, O. Coreño, I. Rodríguez, S. Gutiérrez, Arsenic and fluoride removal from groundwater by electrocoagulation using a continuous filter-press reactor, *Chemosphere*, 144 (2016) 2113–2120.
- [24] L.S. Thakur, P. Mondal, Simultaneous arsenic and fluoride removal from synthetic and real groundwater by electrocoagulation process: parametric and cost evaluation, *J. Environ. Manage.*, 190 (2017) 102–112.
- [25] S. Aoudj, A. Khelifa, N. Drouiche, Removal of fluoride, SDS, ammonia and turbidity from semiconductor wastewater by combined electrocoagulation–electroflotation, *Chemosphere*, 180 (2017) 379–387.
- [26] F. Belkessama, H. Lounicib, N. Drouichec, M. Aidenea, R. Sonid, Removal of toxic metal Cr(VI) from aqueous solutions by electrocoagulation using aluminum electrodes, *Desal. Water Treat.*, 86 (2017) 221–230.
- [27] O. Sahu, B. Mazumdar, P.K. Chaudhari, Treatment of wastewater by electrocoagulation: a review, *Environ. Sci. Pollut. Res.*, 21 (2014) 2397–2413.
- [28] J.N. Hakizimana, B. Gourich, M. Chafi, Y. Stiriba, C. Vial, P. Drogui, J. Naja, Electrocoagulation process in water treatment: a review of electrocoagulation modeling approaches, *Desalination*, 404 (2017) 1–21.
- [29] M. Changmai, M. Pasawan, M.K. Purkait, A hybrid method for the removal of fluoride from drinking water: parametric study and cost estimation, *Sep. Purif. Technol.*, 206 (2018) 140–148.
- [30] A. Betancor-Abreu, V.F. Mena, S. González, S. Delgado, R.M. Souto, J.J. Santana, Design and optimization of an electrocoagulation reactor for fluoride remediation in underground water sources for human consumption, *J. Water Process. Eng.*, 31 (2019) 100865.
- [31] E. Sik, M. Kobya, E. Demirbas, E. Gengec, M.S. Oncel, Combined effects of co-existing anions on the removal of arsenic from groundwater by electrocoagulation process: optimization through response surface methodology, *J. Environ. Chem. Eng.*, 5 (2017) 3792–3802.
- [32] APHA, Standard Methods for the Examination of Water and Wastewater, American Public Health Association, Washington, DC, 2012.
- [33] U.T. Un, A.S. Kopalal, U.B. Ogutveren, Fluoride removal from water and wastewater with a batch cylindrical electrode using electrocoagulation, *Chem. Eng. J.*, 223 (2013) 110–115.
- [34] F. Shen, X. Chen, P. Gao, G. Chen, Electrochemical removal of fluoride ions from industrial wastewater, *Chem. Eng. Sci.*, 58 (2003) 987–993.
- [35] K.J. Kim, K. Baek, S. Ji, Y. Cheong, G. Yim, A. Jang, Study on electrocoagulation parameters (current density, pH, and electrode distance) for removal of fluoride from groundwater, *Environ. Earth Sci.*, 75 (2016) 45.
- [36] S. Liu, X. Ye, K. He, Y. Chen, Y. Hu, Simultaneous removal of Ni(II) and fluoride from a real flue gas desulfurization wastewater by electrocoagulation using Fe/C/Al electrode, *J. Water Reuse Desal.*, 7 (2017) 288–297.
- [37] G. Mouedhen, M. Feki, M.D.P. Wery, H.F. Ayedi, Behavior of aluminum electrodes in electrocoagulation process, *J. Hazard. Mater.*, 150 (2008) 124–135.
- [38] N.B. Grich, A. Attour, M.L.P. Mostefa, M. Tlili, F. Lapique, Fluoride removal from water by electrocoagulation with aluminum electrodes: effect of the water quality, *Desal. Water Treat.*, 144 (2019) 145–155.
- [39] N. Drouiche, B. Palahouane, S. Aoudj, M. Hecini, O. Bouchelaghem, T. Ouslimane, Defluoridation of post treated photovoltaic wastewater using aluminum electrodes: optimization of operating parameters and sludge characteristics, *J. Solution Chem.*, 45 (2016) 1571–1579.
- [40] A.L. Valdivieso, J.R. Bahena, S. Song, R.H. Urbina, Temperature effect on the zeta potential and fluoride adsorption at the α -Al₂O₃/aqueous solution interface, *J. Colloid Interface Sci.*, 298 (2006) 1–5.
- [41] W. Yang, X. Dou, Y. Li, D. Mohan, C.U. Pittman, Y.S. Ok, Performance and mass transfer of aqueous fluoride removal by a magnetic alumina aerogel, *RSC Adv.*, 6 (2016) 112988–112999.
- [42] D. Ghosh, C.R. Medhi, M.K. Purkait, Treatment of fluoride containing drinking water by electrocoagulation using monopolar and bipolar electrode connections, *Chemosphere*, 73 (2008) 1393–1400.
- [43] M. Rosales, O. Coreño, J.L. Nava, Removal of hydrated silica, fluoride and arsenic from groundwater by electrocoagulation using a continuous reactor with a twelve-cell stack, *Chemosphere*, 211 (2018) 149–155.
- [44] P. Huestis, C.I. Pearce, X. Zhang, K.M. Rosso, J.A. LaVerne, Radiolytic stability of gibbsite and boehmite with adsorbed water, *J. Nucl. Mater.*, 501 (2018) 224–233.
- [45] H.D. Ruan, R.L. Frost, J.T. Klopogge, Comparison of Raman spectra in characterizing gibbsite, bayerite, diaspore and boehmite, *J. Raman Spectrosc.*, 32 (2001) 745–750.
- [46] R.R. Nazmutdinov, T.T. Zinkicheva, S.Y. Vassiliev, D.V. Glukhov, G.A. Tsirlina, M. Probst, A spectroscopic and computational study of Al(III) complexes in sodium cryolite melts: Ionic composition in a wide range of cryolite ratios, *Spectrochim. Acta, Part A*, 75 (2010) 1244–1252.
- [47] S. Vasudevan, J. Lakshmi, G. Sozhan, Studies on a Mg–Al–Zn alloy as an anode for the removal of fluoride from drinking water in an electrocoagulation process, *Clean Soil Air Water*, 37 (2009) 372–378.

Supplementary information

Table S1

Fluoride levels in groundwater of various districts of Punjab, India as per CGWB report [9]

	District	Block	Location	Latitude (North)	Longitude (East)	Fluoride (mg/L)
1	Ferozpur	Abohar	Bazidpur Bhoma	29.952972	74.381340	9.11
2	Mansa	Mansa	Bhikhi	30.056874	75.530404	7.33
3	Taran Tarn	Bhikiwind	Khalra	31.395699	74.626651	6.35
4	Muktsar	Malout	Kabarwala	30.193664	74.408709	6.05
5	Ferozpur	Faridkot	Dalsinghwala	30.463839	74.928548	6.03
6	Sangrur	Lehraggaga	ChuralKalan	29.823322	75.814849	5.16
7	Bathinda	Phul	Gurusar	30.491374	75.144886	4.50
8	Faridkot	Momdot	Killi	30.845239	74.484388	4.29
9	Muktsar	Lambi	Kuttianwala	30.058582	74.607468	4.28
10	Patiala	Rajpura	Rajpura	30.340092	76.369678	3.50
11	Ferozpur	KhuianSarwar	KhuianSarwar	30.110941	74.066188	3.39
12	Ferozpur	Guruhar	Swahwala	30.602246	74.301846	3.36
13	Ferozpur	Kotkapura	Dhiwankalan	30.574736	74.86102	3.33
14	SAS nagar	DeraBassi	GholuMajra	30.538938	76.819145	2.90
15	Ferozpur	Kotkapura	BajaKhanna	30.456726	74.981018	2.85
16	Moga	Moga	Darapur	30.841734	74.960125	2.43
17	Mansa	Jhunir	Moffar	29.777093	75.419055	2.32
18	Sangrur	Andana	Haryo	29.811929	76.038481	2.18
19	Bathinda	Bathinda	Gulabgarh	30.108750	75.091000	2.16
20	Ferozpur	Kotkapura	Matta	30.483701	74.836577	1.95
21	Sangrur	Andana	Bulan	29.763132	76.007803	1.91
22	Mansa	Mansa	Ralla	30.117488	75.430238	1.83
23	Bathinda	Rampura	Kotha Guru	30.495070	75.095909	1.59



Fig. S1. Skeletal and dental fluorosis among inhabitants of Khalra village, Tarn Taran, Punjab.

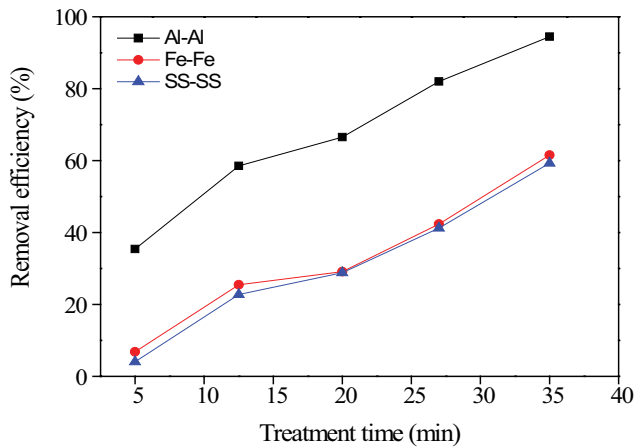


Fig. S2. Effect of electrode material on fluoride removal efficiency (pH = 7, current density = 10 A/m², and simulated fluoride = 5 mg/L).

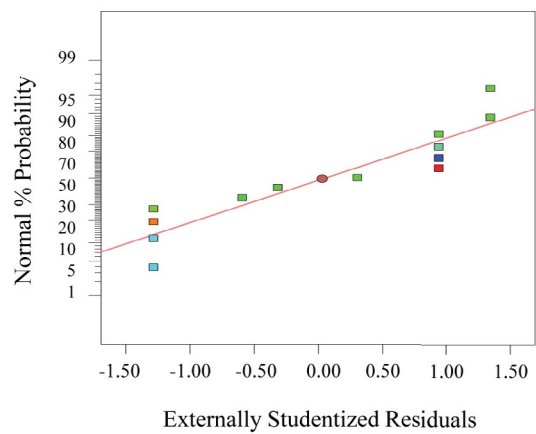


Fig. S3. Normal % probability plot showing the effect of treatment time and current density on fluoride removal efficiency.

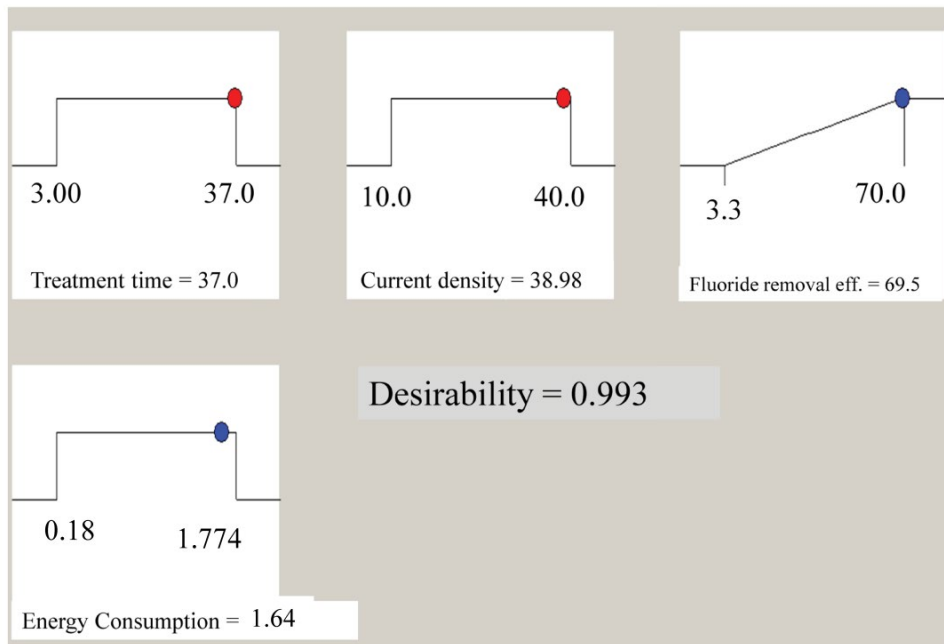


Fig. S4. Desirability plot showing optimum process conditions for single step defluoridation process.

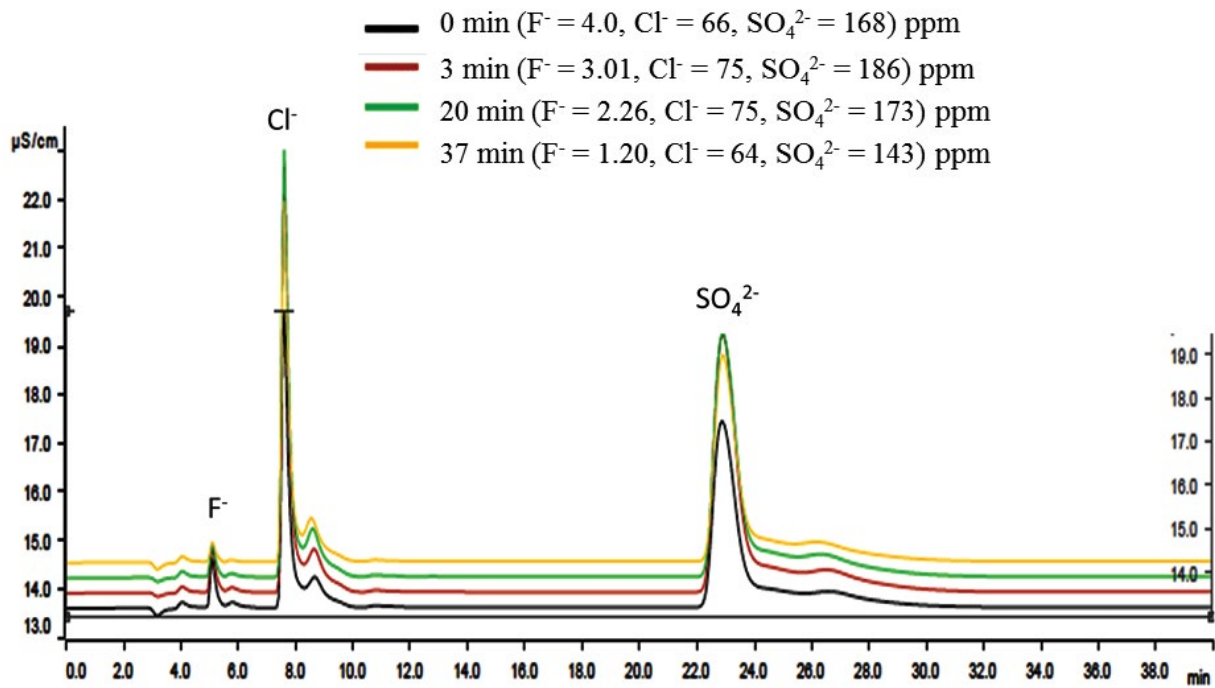


Fig. S5. Chromatogram showing overlay plot at different treatment time.